Bulletin of the Seismological Society of America, Vol. 100, No. 3, pp. 1356–1362, June 2010, doi: 10.1785/0120090299

Short Note

Temporal Variations in Crustal Scattering Structure near Parkfield, California, Using Receiver Functions

by Pascal Audet

Abstract We investigate temporal variations in teleseismic receiver functions using 11 yr of data at station PKD near Parkfield, California, by stacking power spectral density (PSD) functions within 12-month windows. We find that PSD levels for both radial and transverse components drop by ~5 dB following the 2003 San Simeon (M 6.5) earthquake, with a persistent reduction in background levels of ~2 dB, relative to the pre-2003 levels, after the 2004 Parkfield (M 6) earthquake, corresponding to an estimated decrease in shear-wave velocity of ~0.12 and ~0.06 km/sec, respectively, or equivalent negative changes in Poisson's ratio of ~0.02 and ~0.01. Our results suggest that the perturbation originates at middle to lower crustal levels, possibly caused by the redistribution of crustal pore fluids, consistent with increased and sustained tremor activity near Parkfield following both earthquakes. This study shows that we can resolve temporal variations in crustal scattering structure near a major seismogenic fault using the receiver function method.

Introduction

Changes in seismic velocities measure changes in the density and elastic moduli of rocks that are a function of a number of intrinsic lithological, as well as extrinsic (e.g., pressure, temperature, pore-fluid pressure), and structural (e.g., cracks, porosity) parameters. Consequently, measuring temporal variations in velocities can be used to infer changes in the conditions under which they occur (e.g., dilatancy [Nur, 1971; Scholz, 1974] or damage [Vidale and Li, 2003]). Typical crustal targets are fault zones, magma chambers, hydrocarbon reservoirs, and landslides. The techniques used to characterize such variations range from repeated seismic experiments (e.g., Husen and Kissling, 2001) to interferometric approaches (e.g., Brenguier, Shapiro, *et al.*, 2008).

One method that provides accurate point measurements of crustal velocity structure is based on the characterization of body-wave scattering beneath a recording broadband station using a collection of teleseismic events, that is, the so-called P-receiver function method. This technique is based on deconvolution of the source time function, approximated by the P-wave train, from the S components of motion. Resulting seismograms represent an approximation to the Earth's impulse response, or Green's function (Bostock, 2007), and are used to determine the geometry and velocity of discrete planar layers. Accuracy is controlled mainly by event coverage within the epicentral distance range 30–100°. Because major earthquakes ($M > 5.5$) mostly occur along plate boundaries, spatial coverage is highly uneven at any given station, resulting in a biased sampling of the crust. In contrast, coverage is fairly regular in time with more than 100, $M > 5.5$ earthquakes occurring annually. At permanent broadband stations with long recording history (> 5 yr), several hundred earthquakes illuminate the same crustal volume quasicontinuously. The repeatability of ray path coverage is similar in principle to successive structural studies; consequently, this technique has the potential to resolve temporal variations in crustal velocity structure.

In this paper we investigate time dependence of receiver functions using data from a permanent broadband station (PKD) near Parkfield, California (Fig. 1). This station has been in operation since 1996 and is located ~3 km southwest of the San Andreas fault (SAF; Fig. 1), close to the transition from the locked segment to the southeast, and close to the creeping section to the northwest. This region is characterized by the recurrence of M ~6 crustal earthquakes every 22 ± 5 yr. The recent occurrence of the nearby 2003 (M 6.5) San Simeon and 2004 (M 6) Parkfield earthquakes provides a unique opportunity to examine temporal variations in crustal scattering structure near a major seismogenic fault.

Previous studies using standard application of receiver functions documented a complex structure beneath station PKD and the existence of a 6 km thick, lower-crustal low-velocity layer with strong (15%) anisotropy (Ozacar and Zandt, 2009). Crustal multiples indicate a 26 km thick crust with average V_P/V_S of 1.88 with slightly lower values (1.83)

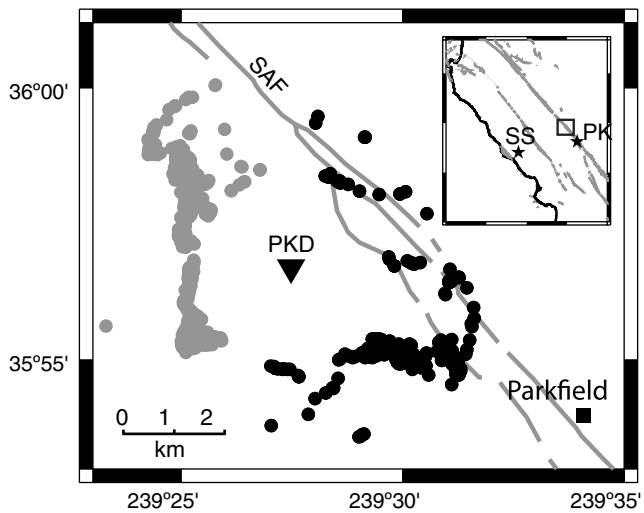

Figure 1. Moho piercing points of receiver functions grouped in two back-azimuth ranges of incoming wave fields (black, 0–200°; gray, 225–360°) at station PKD near Parkfield, California, with respect to study region (inset, major faults in gray). This grouping also corresponds to sampled volumes exhibiting different contrasts in V_P/V_S of the upper to middle crust with lower values in the west. SAF is indicated by the gray lines near Parkfield. Stars in the inset indicate the location of the 2003 San Simeon (SS) and 2004 Parkfield (PK) earthquakes.

for the upper and middle crust in the west. To explore temporal variations in crustal structure, we collect seismograms for 1108 events with $M > 5.7$ that occurred between January 1997 and December 2008 at the requisite epicentral distance. Event coverage is dominated by the western Pacific, Fiji-Tonga, and Central and South America subduction zones. Back-azimuthal coverage is good from 0–200° with 284 events sampling the crust south and east of the SAF in a direction mostly parallel to fault strike and from 225 to 360° with 824 events sampling the crust west of the SAF (Fig. 1).

Method and Results

Prior to receiver function processing, seismograms are rotated to the P, S_V (radial), and S_H (transverse) wave modes using the free surface transfer matrix (Bostock, 1998). The receiver function method employs the P component as an estimate of the source to deconvolve the S_V and S_H components and recover P-to-S wave conversions from velocity discontinuities beneath a recording station. This procedure involves calculating the spectral ratio R between individual, single-event P and S seismograms,

$$R(\omega) = \frac{S(\omega)P^*(\omega)\Phi(\omega)}{|P(\omega)|^2}, \tag{1}$$

where ω is the angular frequency, Φ is a regularizing filter to avoid contamination by noise, the asterisk ($*$) indicates complex conjugation, and S can be either S_V or S_H. The filter Φ can be calculated from the damped least-squares deconvolution solution,

$$\Phi(\omega) = \frac{|P(\omega)|^2}{|P(\omega)|^2 + \delta},$$

where δ is a constant determined by standard optimization schemes based on preevent noise variance on the P component (Bostock, 2007). Deconvolution based on this filter is similar to water-level deconvolution. Because δ is a constant, this approach implicitely assumes random (white) noise. However, the seismic noise spectrum is not flat at frequencies of interest due to microseismic peaks, and varies seasonally as a result of increased storm activity in the winter (McNamara and Bulland, 2004). The water-level filter does not capture the frequency dependence of microseismic noise that can be mapped back into the receiver functions and produce bias. This effect is usually dealt with by selecting events with high signal-to-noise ratios (effectively discarding most events occurring in winter), postdeconvolution band-pass filtering, and stacking to improve coherency of scattered signals. Because we are interested in recovering small perturbations of the Green's function with time, deconvolution using a water-level filter is not appropriate.

In order to reduce the effect of noise in the deconvolution, we use a Wiener filtering approach. The Wiener filter is optimally designed to produce a signal that is as close as possible to the uncorrupted signal in the least-squares sense (Press *et al.*, 1992). In Wiener filtering the regularizing parameter is directly estimated from the preevent noise spectrum, reducing bias to a minimum. Most implementations of the Wiener filter in receiver function studies consider only preevent noise on the P component. Because the angle of incidence of teleseismic P waves at the surface is small (slowness of 0.04–0.08 sec/km), the P-component preevent noise is dominated by vertical motion. Noise levels on horizontal components can differ by up to 10 dB from the vertical component and have different sensitivities to climatic perturbations that cause ground tilting (e.g., winds, barometric pressure, precipitation) (Beauduin *et al.*, 1996). To mitigate this effect, we devise an *ad hoc* Wiener filter for receiver functions derived from the auto- and covariance of noise on multiple channels:

$$\Phi(\omega) = \frac{|P(\omega)|^2}{|P(\omega)|^2 + [\frac{1}{4}|N_P(\omega)|^2 + \frac{1}{4}|N_S(\omega)|^2 + \frac{1}{2}|N_P^*(\omega)N_S(\omega)|]}, \tag{2}$$

where N_P and N_S are preevent noise on the P and S components, respectively. Using this filter we calculate single-event receiver functions for all teleseismic events recorded at station PKD (Fig. 1).

The decrease in seismic velocity is expected to be relatively small, and standard processing of the time-domain receiver function is unlikely to resolve such small perturbation. However, because the spectral content of deconvolved, unfiltered receiver functions represents the magnitude and

phase of the scattering structure, analyzing the squared modulus (i.e., power spectral density [PSD]) can provide an estimate of the scattering energy as a function of frequency. Thus, instead of inverse Fourier transforming equation (1) to obtain the time-domain response, we calculate the PSD for each individual, unfiltered receiver function using the multitaper method (Prieto *et al.*, 2009). Because we are interested in crustal scattering structure, we calculated the PSD of the first 30 sec for each receiver function. To further reduce variance of the estimates we resample the PSDs in full-octave period averages taken at 1/8 octave intervals (McNamara and Bulland, 2004). We subsequently collect and stack the PSDs within 95% overlapping, 12-month segments using the median to improve stack coherency (Figs. 2 and 3). We found that averaging within 12-month bins offered the best compromise between temporal resolution and variance reduction and assigned the resulting PSD stack to the central date within each bin. Spectral power is calculated for each component by integrating the PSDs between 0.5 and 3 sec, where energy is at a maximum.

We collected the PSD time series into two groups according to back azimuth of the incoming wave field to reflect the difference in crustal structure observed in a previous study (Ozacar and Zandt, 2009). Results show a clear drop of ~5 dB in PSD level around the time of the 2003 M 6.5 San Simeon earthquake with a subsequent persistent reduction (~2 dB) in the postseismic background PSD level relative to pre-2003 event (Fig. 2a–c). The exact start time of the observed change in PSD appears to lead the San Simeon event by ~6 months; however this is due to the smoothing effect of stacking within 12-month bins. Assigning PSD stacks to the end date within each bin would shift the values forward by 6 months, effectively erasing the apparent lead time of the drop in PSD. Interestingly, the change is observed only for events coming from the back-azimuth range 0–200° (compare Figs. 2 and 3), dominated by events originating from South–Central America, which sample the crust along strike and southwest of the SAF near Parkfield (Fig. 1) and closer to the area of rupture of the 2004 event. Narrowing the angular aperture within the range 0–200° does not significantly change the result, indicating that the entire volume of crust sampled by these events responded to stress perturbations caused by the earthquakes.

Spatiotemporal sampling does not appear to be biased by source distribution within the 0–200° back-azimuth range (Fig. 2d,e). We investigate stability in instrument response by collecting 100 sec preevent noise records for each event that are rotated into P, S_V, and S_H coordinates to facilitate comparison with receiver function results. Spectral response is evaluated by calculating the PSD and transfer functions (admittance and coherence) of P and S_V components of ground noise, which are resampled and stacked using the same procedure described previously (Fig. 4). This analysis shows that the instrument was stable over the entire period analyzed.

Discussion

Variations in PSD levels do not constrain the extent of the perturbation; however, given its azimuthal dependence, it is unlikely that it originates at shallow levels. Its manifestation at periods of 0.5–3 sec where PSD is highest also suggests a depth-integrated effect. Ignoring density changes, reduced PSD levels imply a decrease in scattering energy (i.e., an increase in scattering attenuation) from velocity perturbations. We approximate the scattered energy as arising from such perturbations in a stochastic medium (e.g., Hong and Kennett, 2003) and write

$$\langle |u^{PS}|^2 \rangle \propto |\xi|^2, \tag{3}$$

where u^{PS} is the scattered wave field from plane P-to-S converted waves, ξ is the spectrum of perturbations in the elastic medium given by $\xi = \delta V_S / V_S$, where V_S is shear-wave velocity, and the brackets indicate ensemble averaging. From this relation we can estimate the change in shear perturbation from a drop of x dB in PSD level:

$$\frac{\langle |u_2^{PS}|^2 \rangle}{\langle |u_1^{PS}|^2 \rangle} = \frac{|\xi + \delta\xi|^2}{|\xi|^2} = 10^{-x/10}, \tag{4}$$

where $\langle |u_1^{PS}|^2 \rangle \propto |\xi|^2$ is the preevent scattered wave field, and $\langle |u_2^{PS}|^2 \rangle \propto |\xi + \delta\xi|^2$ is the postearthquake wave field. Assuming background shear velocity β of 3 km/sec and perturbations ξ on the order of 10^{-1}, the variations in PSD correspond to reductions of β of ~0.12 and ~0.06 km/sec, respectively, for the San Simeon and Parkfield events. Using an average V_P/V_S of 1.88 for the crust (Ozacar and Zandt, 2009) and assuming that the P velocity remained constant, the changes in shear velocity correspond to a reduction in V_P/V_S of ~0.08 and ~0.04 with respect to preearthquake values or an equivalent decrease in Poisson's ratio of ~0.02 and ~0.01. These results are consistent with values obtained from ambient noise correlation studies near Parkfield (Brenguier, Campillo, *et al.*, 2008), where 0.04% and 0.08% reductions in velocity were found after the San Simeon and Parkfield earthquakes, respectively. Brenguier, Campillo, *et al.* (2008) interpreted their results as a combination of nonlinear ground motion in the shallow layer with rapid recovery to background values and longer postseismic stress relaxation within the deeper parts of the fault zone and surrounding region. Our measurements indicate that the San Simeon earthquake, located ~65 km to the southwest of station PKD, had a stronger effect on velocity perturbation than the nearby Parkfield event, which possibly reflects differences in depth sensitivity between the two methods. Noise correlations at 0.1–0.9 Hz are mainly sensitive to the upper ~10 km within the crust. The azimuthal dependence of receiver function results suggests that at least parts of the middle to lower crust also exhibit velocity changes, which implies a deep source of velocity perturbations. The increase in tremor activity near Parkfield following the 2003 and 2004 events, occurring below the seismogenic part of the fault, is consistent with

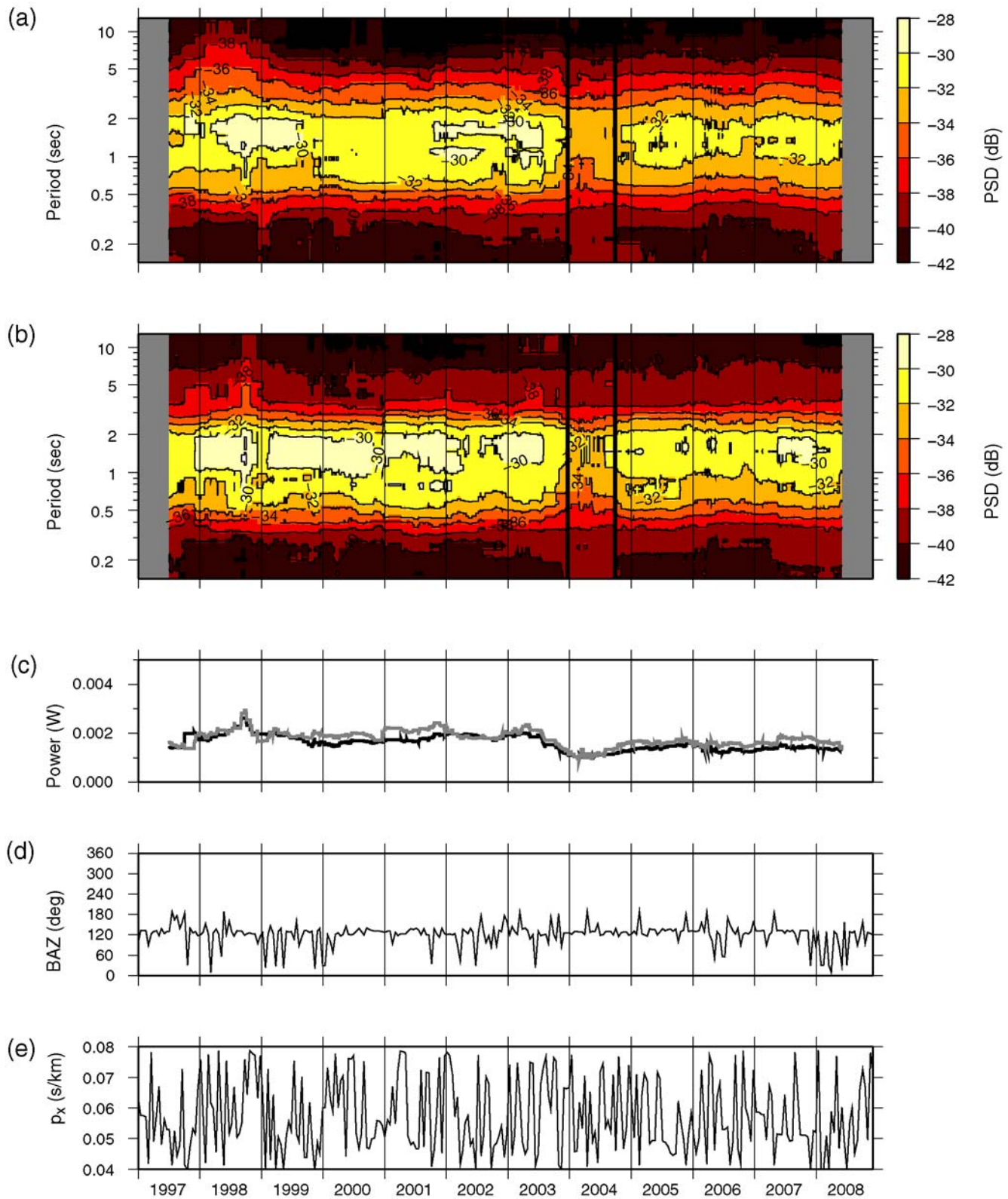

Figure 2. Temporal variations in receiver functions at station PKD for back azimuths 0–200°. Top panels show PSD of receiver functions binned within 95% overlapping, 12-month windows for (a) radial and (b) transverse components. (c) Corresponding variations in total power (black line, radial; gray line, transverse). Distribution of the 284 events with respect to (d) back azimuth and (e) slowness of incoming wave fields is presented in bottom panels. The thick vertical lines in (a) and (b) indicate times of the San Simeon (2003) and Parkfield (2004) earthquakes. The color version of this figure is available only in the electronic edition.

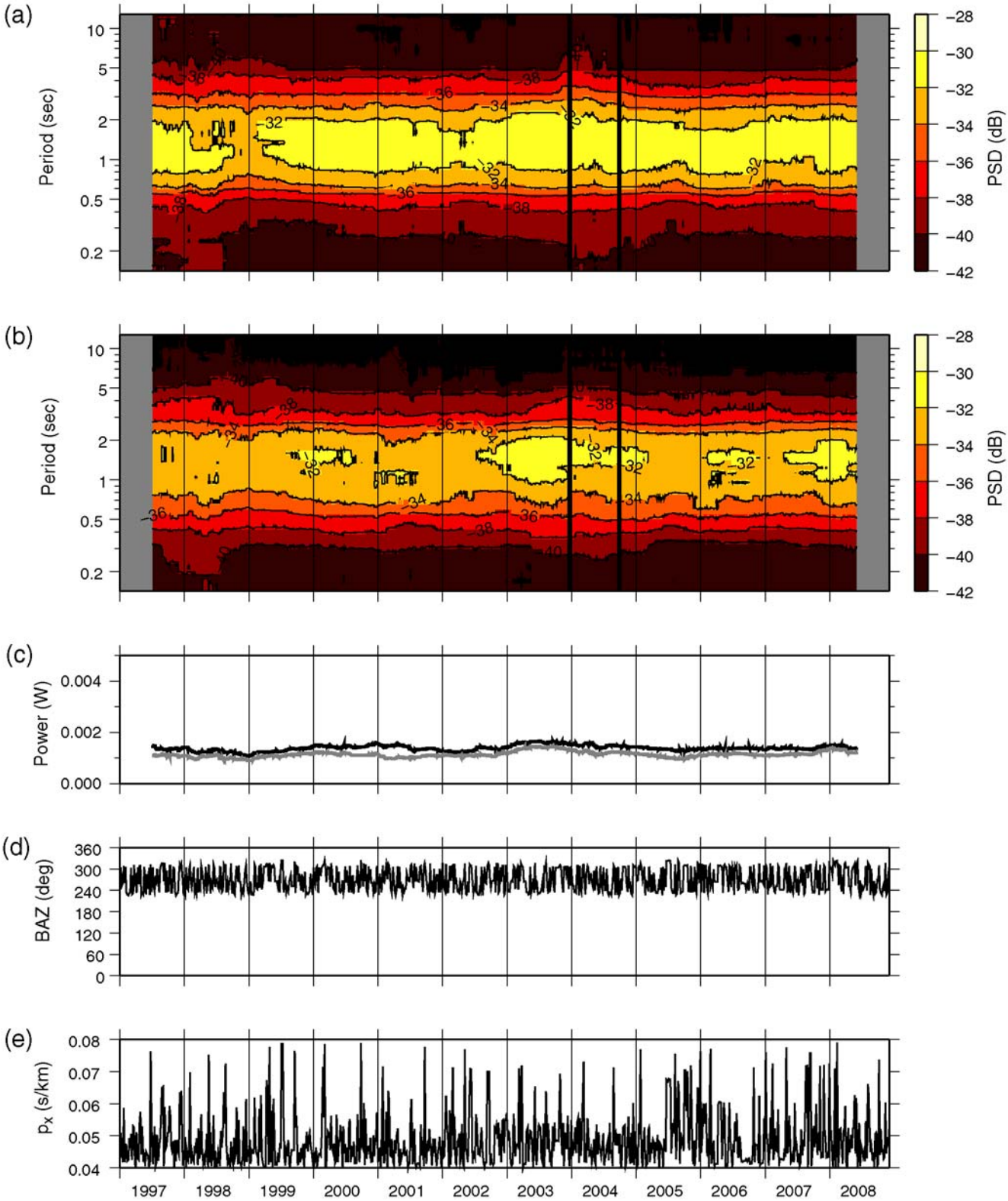

Figure 3. Same as Figure 2 for 824 events with back azimuths. The color version of this figure is available only in the electronic edition.

a perturbation originating near the base of the crust (Nadeau and Guilhem, 2009).

Although the source of the perturbation is unknown, it is consistent with redistribution of crustal pore fluids and the breaking of impermeable barriers due to shaking (Elkhoury *et al.*, 2006) near the SAF zone after the San Simeon earthquake. The fact that the Parkfield earthquake, which caused much larger shaking near station PKD, did not have a

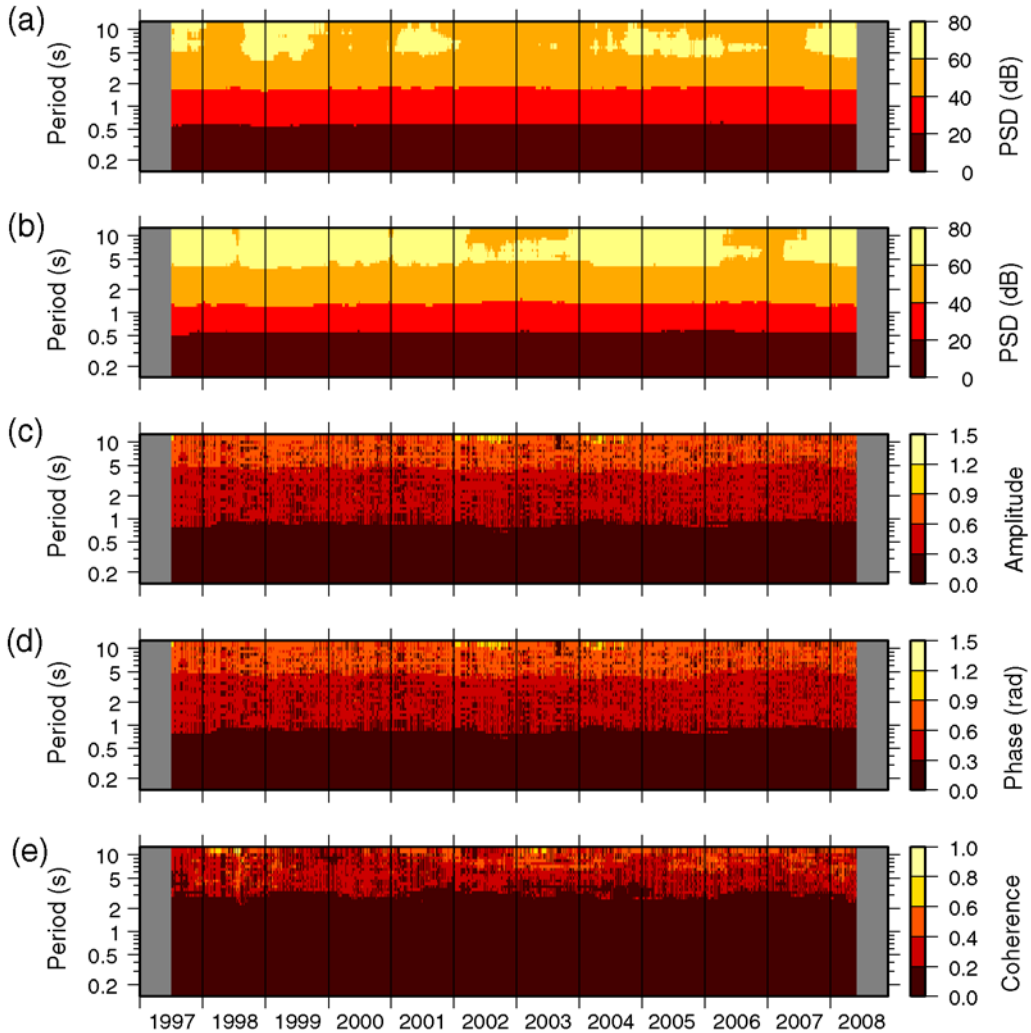

Figure 4. Instrument response calculated from preevent noise measurements on rotated components in the P–S_V system. (a) and (b) PSD levels for the P and S_V components of noise, respectively. Flatness in the (c) amplitude and (d) phase of the linear transfer function and the (e) coherence between both noise components gives an indication of instrument stability. The color version of this figure is available only in the electronic edition.

similarly strong effect on the PSD levels may reflect the partial, and spatially limited, reequilibration of pore-fluid pressures in the crustal column after the San Simeon event. The increased and sustained tremor activity after the Parkfield earthquake is also consistent with a deep fluid source and suggests a shift in the deformation process and stress accumulation beneath this portion of the SAF (Nadeau and Guilhem, 2009).

Conclusion

We use 11 yr of data at station PKD near Parkfield, California, to examine temporal variations in crustal scattering structure using a novel application of receiver functions. We find a significant drop in PSD levels (~5 dB) of scattered wave fields following the 2003 San Simeon, California, earthquake, and recovery to reduced levels (~2 dB) thereafter. We estimate the changes in PSD to be caused by both sudden and persistent reductions in S velocity of ~0.12 and ~0.06 km/sec, respectively, or equivalent changes in Poisson's ratio of ~0.02 and ~0.01. This result suggests that dynamic strain may possibly play a role in the redistribution of deep crustal pore fluids. Improved understanding of the source of these changes may be addressed by using complementary methods that provide depth resolution and by using different data sets. This study indicates that the receiver function method bears the potential for investigating 4D faulting processes.

Data and Resources

Station PKD is part of the Berkeley Digital Seismic Network (BDSN), and data were made available by the Northern California Earthquake Data Center (NCEDC). Information on data used in this study can be found at the following Web

address: http://seismo.berkeley.edu/seismo.networks.html (last accessed September 2009).

Acknowledgments

The author acknowledges insightful reviews by B. H. Jacobsen and discussions with M. Bostock, R. Bürgmann, and M. Manga. This work was supported by the Miller Institute for Basic Research in Science (UC Berkeley).

References

Beauduin, R., P. Lognonné, J. P. Montagner, S. Cacho, J. F. Karczewski, and M. Morand (1996). The effects of the atmospheric pressure changes on seismic signals, or how to improve the quality of a station, *Bull. Seismol. Soc. Am.* **86,** 1760–1769.

Bostock, M. G. (1998). Mantle stratigraphy and evolution of the Slave province, *J. Geophys. Res.* **103,** 21,183–21,200.

Bostock, M. G. (2007). Regional methods, in *Seismology and Structure of the Earth*, G. Schubert (Editor), Vol. **1** of Treatise on Geophysics, Elsevier, Amsterdam, 219–246.

Brenguier, F., M. Campillo, C. Hadziioannou, N. M. Shapiro, R. M. Nadeau, and E. Larose (2008). Postseismic relaxation along the San Andreas fault at Parkfield from continuous seismological observations, *Science* **321,** 1478–1481, doi 10.1126/science.1160943.

Brenguier, F., N. M. Shapiro, M. Campillo, V. Ferrazzini, Z. Duputel, O. Coutant, and A. Nercessian (2008). Towards forecasting volcanic eruptions using seismic noise, *Nat. Geosci.* **1,** 126–130, doi 10.1038/ngeo104.

Elkhoury, J. E., E. E. Brodsky, and D. Agnew (2006). Seismic waves increase permeability, *Nature* **441,** 1135–1138.

Hong, T.-K., and B. L. N. Kennett (2003). Scattering attenuation of 2D elastic waves: Theory and numerical modeling using a wavelet-based method, *Bull. Seismol. Soc. Am.* **93,** 922–938.

Husen, S., and E. Kissling (2001). Postseismic fluid flow after the large subduction earthquake of Antofagasta, Chile, *Geology* **29,** 847–850.

McNamara, D. E., and R. P. Bulland (2004). Ambient noise levels in the continental United States, *Bull. Seismol. Soc. Am.* **94,** 1517–1527.

Nadeau, R. M., and A. Guilhem (2009). Nonvolcanic tremor evolution and the San Simeon and Parkfield, California, earthquakes, *Science* **325,** 191–193.

Nur, A. (1971). Effects of stress on velocity anisotropy in rocks with cracks, *J. Geophys. Res.* **76,** 2022–2034.

Ozacar, A. A., and G. Zandt (2009). Crustal structure and seismic anisotropy near the San Andreas fault at Parkfield, California, *Geophys. J. Int.* **178,** 1098–1104, doi 10.1111/j.1365246X.2009.04198.

Press, W. H., S. A. Teukolsky, W. T. Vetterling, and B. P. Flannery (1992). *Numerical Recipes in FORTRAN: The Art of Scientific Computing*, Second Ed., Cambridge U Press, New York.

Prieto, G. A., R. L. Parker, and F. L. Vernon (2009). A Fortran 90 library for multitaper spectrum analysis, *Comput. Geosci.* **35,** 1701–1710.

Scholz, C. H. (1974). Post-earthquake dilatancy recovery, *Geology* **2,** 551–554.

Vidale, J. E., and Y. G. Li (2003). Damage to the shallow Landers fault the nearby Hector Mine earthquake, *Nature* **421,** 524–526.

Berkeley Seismological Laboratory
University of California Berkeley
377 McCone Hall
Berkeley, California 94720-4767
paudet@berkeley.edu

Manuscript received 11 September 2009